

PAPER

Optimal planar leg geometry in robots and crabs for idealized rocky terrain

To cite this article: Yang Chen *et al* 2022 *Bioinspir. Biomim.* **17** 066009

View the [article online](#) for updates and enhancements.

You may also like

- [Sideways crab-walking is faster and more efficient than forward walking for a hexapod robot](#)
Yang Chen, John E Grezmaek, Nicole M Graf *et al.*
- [Analyzing complex wake-terrain interactions and its implications on wind-farm performance.](#)
Mandar Tabib, Adil Rasheed and Franz Fuchs
- [An insect-scale robot reveals the effects of different body dynamics regimes during open-loop running in feature-laden terrain](#)
Perrin E Schiebel, Jennifer Shum, Henry Cerbone *et al.*

Bioinspiration & Biomimetics



PAPER

Optimal planar leg geometry in robots and crabs for idealized rocky terrain

RECEIVED
31 March 2022

REVISED
30 June 2022

ACCEPTED FOR PUBLICATION
1 September 2022

PUBLISHED
11 October 2022

Yang Chen¹ , Glenna Clifton², Nicole M Graf¹ , Kayla Durand², Jennifer Taylor³, Yifeng Gong¹, John E Grezma¹ and Kathryn A Daltorio^{1,*}

¹ Department of Mechanical and Aerospace Engineering, Case Western Reserve University, Cleveland, OH, United States of America

² Biology Department, University of Portland, Portland, OR, United States of America

³ Marine Biology Research Division, Scripps Institution of Oceanography, UC San Diego, CA, United States of America

* Author to whom any correspondence should be addressed.

E-mail: yxc1280@case.edu, cliftong@up.edu, nmg63@case.edu, durand24@up.edu, j3taylor@ucsd.edu, yxg553@case.edu, jeg100@case.edu and kathryn.daltorio@case.edu

Keywords: sideways walking, *Hemigrapsus nudus*, *Pachygrapsus crassipes*, amphibious crab robots, leg design optimization, grasping uneven terrain, distributed inward gripping

Supplementary material for this article is available [online](#)

Abstract

Natural terrain is uneven so it may be beneficial to grasp onto the depressions or ‘valleys’ between obstacles when walking over such a surface. To examine how leg geometry influences walking across obstacles with valleys, we (1) modeled the performance of a two-linkage leg with parallel axis ‘hip’ and ‘knee’ joints to determine how relative segment lengths influence stepping across rocks of varying diameter, and (2) measured the walking limbs in two species of intertidal crabs, *Hemigrapsus nudus* and *Pachygrapsus crassipes*, which live on rocky shores and granular terrains. We idealized uneven terrains as adjacent rigid hemispherical ‘rocks’ with valleys between them and calculated kinematic factors such as workspace, limb angles with respect to the ground, and body configurations needed to step over rocks. We first find that the simulated foot tip radius relative to the rock radius is limited by friction and material failure. To enable force closure for grasping, and assuming that friction coefficients above 0.5 are unrealistic, the foot tip radius must be at least 10 times smaller than that of the rocks. However, ratios above 15 are at risk of fracture. Second, we find the theoretical optimal leg geometry for robots is, with the distal segment 0.63 of the total length, which enables the traversal of rocks with a diameter that is 37% of the total leg length. Surprisingly, the intertidal crabs’ walking limbs cluster around the same limb ratio of 0.63, showing deviations for limbs less specialized for walking. Our results can be applied broadly when designing segment lengths and foot shapes for legged robots on uneven terrain, as demonstrated here using a hexapod crab-inspired robot. Furthermore, these findings can inform our understanding of the evolutionary patterns in leg anatomy associated with adapting to rocky terrain.

1. Introduction

While wheeled robots are more efficient on smooth and flat surfaces, legs enable the traversal of rocky [1–3], sandy [4–6], and other natural terrains [7–17]. Walking with legs creates a trade-off. Using more limbs provides greater stability, but also increases control complexity and weight. One way to improve stability while moving over uneven terrain without adding additional legs involves strategically placing the legs to generate horizontal ground reaction forces. Here we investigate how leg design influences the act

of stepping over hemispherical rocks and into the enclosed ‘valleys.’

Since robots are worse at ‘getting back on their feet’ than animals, an important consideration for legged robots is keeping the robot upright. Stability for legged robots is typically characterized based on the location of the center of mass (COM) relative to the support polygon [18, 19]. The support polygon is defined as the closed shape that connects the feet in stance (aka the feet on the ground). If the COM is outside the polygon (e.g. the robot leans too far away from the feet) the moment of the weight is destabilizing (e.g. the robot starts to tip and fall).

In contrast, if the weight is centered between the legs, the robot is considered stable (the body weight cannot tip the robot). However, this heuristic for stability is insufficient if the weight vector does not point ‘down’ relative to the robot, or if there are other destabilizing forces that are large relative to the weight. Examples include steep surface climbing (where gravity direction is not normal to ground), microgravity environments (where weight is small), surf zones (where hydrodynamic forces are large) and in manipulation tasks which can create large forces relative to the body weight of the robot. Robots face increased stability challenges on uneven terrains, which may cause the robot body to tilt, limiting foot placement and therefore restricting the support polygon.

A benefit of non-flat terrain is that it provides ‘valleys’ created by surface features, which could be exploited to ‘grab the ground’. Grasping the ground enables the legs to apply larger ground reaction forces and increases the horizontal component of these forces, improving stability and maneuverability. However, utilizing these valleys restricts the positioning of the legs, potentially trapping the robot if it is unable to reposition a leg to another foothold. Consider crossing a rocky riverbed—most people look for smooth flat stepping stones to avoid slipping or twisting an ankle. Robots can do this too, with good mapping and planning algorithms [1] or with trial and error [20]. However, if the flat footholds become farther apart, one must either risk longer (and sometimes dynamic) steps or step in between the obstacles. Stepping into a valley requires a more vertical position of the distal leg segment. Stepping in a valley at the wrong angle could lead to mechanical fracture.

Thus, there is a fundamental divide between robots that are designed to use flat footfall locations and those specialized for finding substrate valleys, which has been investigated most in climbing robots. The most efficient climbing robots keep the body close to the substrate maximizing the search area for concave footholds in the robot’s horizontal plane [14–17]. Climbing robots address similar problems and demonstrate advantages of seeking concave footholds. For example, rather than large ‘valleys’, some vertical surfaces are planar (aka appear flat from far away), but at smaller scales have frequent concavities. Robots can passively seek these concavities to use as footholds by moving feet tangentially along flat but not smooth surfaces until a foot catches, to climb vertical rock, stucco, screens and more [14–17]. Fine spines increase the frequency of usable footholds, and if many spines are used in parallel, even large loads can be distributed so as not to exceed the asperity strength [21, 22]. Other rock climbing robots have demonstrated the ability to carefully plan to use challenging handholds like human rock climbers [11–13]. Since keeping the COM close to the climbing

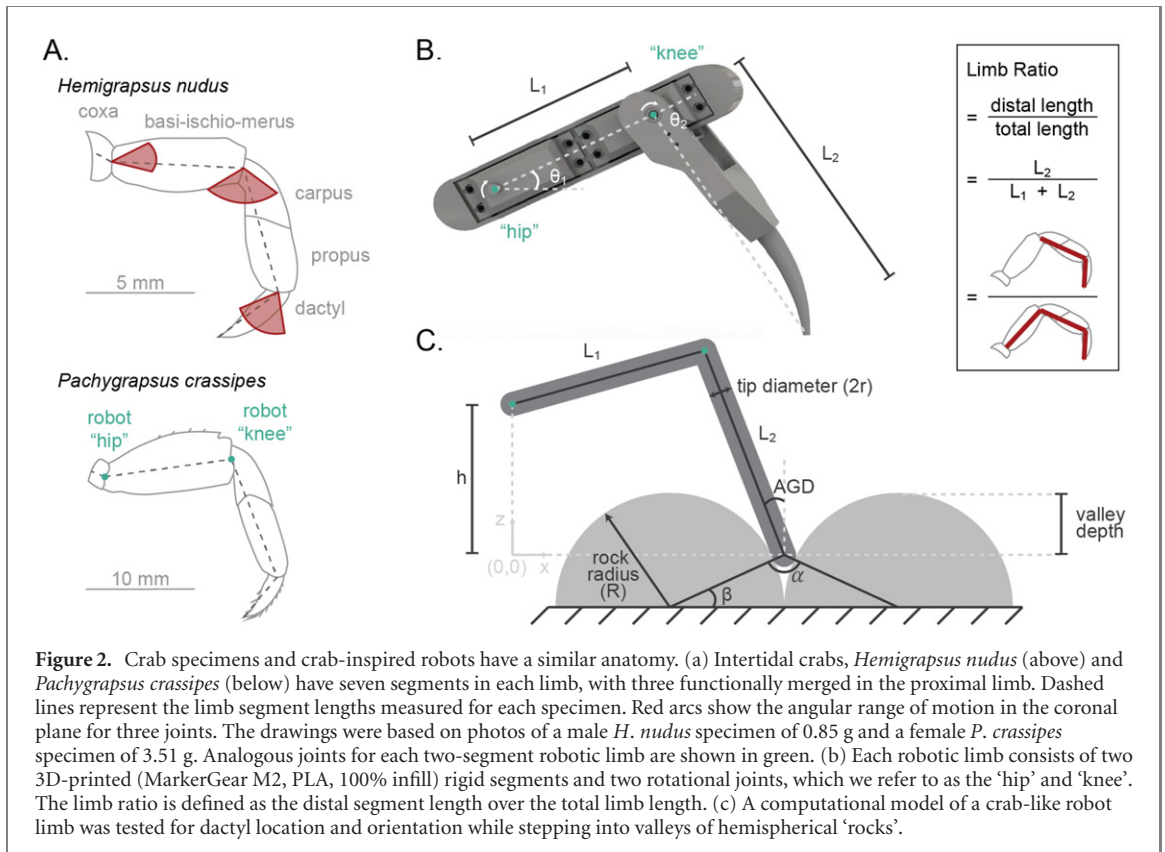
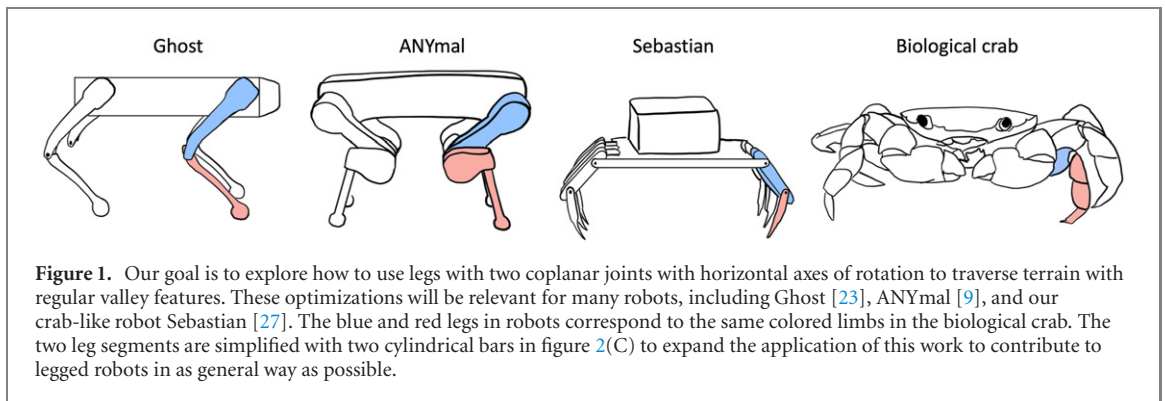
surface reduces pitch-back, the feet have a wide range of motion in the frontal plane, but have comparatively less range of motion in the sagittal plane. In other words, climbing robots have distinctly flatter overall shapes than most walking robots. Specifically, when rotational axes of the joints are vertical, the ability to address out-of-plane unevenness is limited. As the distance between concavities approaches the maximum step size, gaits and leg designs will need to be optimized to maximize the degree of unevenness that the robot can traverse.

Robots designed to walk over uneven terrain often possess four or more legs, each with at least two coplanar joints that pivot around a horizontal axis of rotation, figure 1. For example, dog-inspired robots like ANYmal [8] or Ghost [23], which are currently being used for inspection tasks, have sagittal plane legs. While simpler nonarticulated leg designs are possible, for example [16, 24–26], these wheel-like legs cannot choose footholds. (Note that sprawled-posture lizards and forward-walking insects have different joint configurations.)

Unlike robots that often move through relatively predictable, human-engineered environments, animals contend with ever-changing and highly variable terrain. Crustaceans range in body size, body plan, and locomotion style, establishing them as a potential inspiration for legged robotics. ‘Intertidal’ crabs that live in the tidal zone regularly contend with uneven, rocky terrain and strong perturbations from waves, which easily destabilize robots [28]. Despite these challenges, crabs successfully navigate tidal zones to evade predators, find shelter in rocky crevices, and acquire food [29, 30]. A crab-like body plan and terrestriality have evolved several times independently [31–35], with some crab species walking both forward and backward, while most primarily move sideways [36]. In multiple instances, forward walking animals have developed a sideways-walking crab-like anatomy in a process called carcinization [33]. These side-walking crabs walk with some pereopods (walking legs) positioned in a mostly 2D orientation in the coronal plane [36]. The planar motion of these limbs resembles that of simple robotic limbs and therefore may inform effective design principles [37]. Since sideways walking has also been shown to enable faster walking for both biological crabs and crab-inspired robots [27, 33], sideways-walking crabs provide valuable inspiration for legged robotics on uneven terrain.

Given the growing need for robots capable of walking on rocky substrates, this study aims to understand how limb geometry influences the kinematic requirements for stepping in valleys between smooth objects.

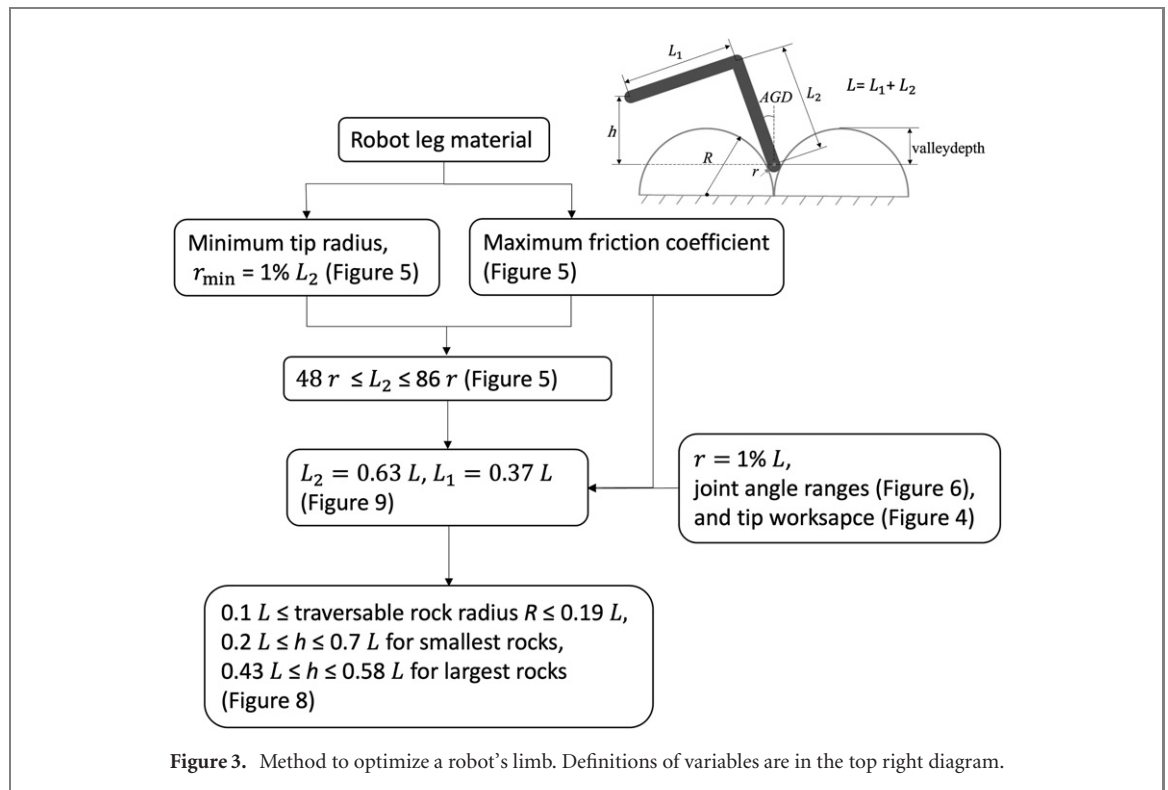
Our intent is to provide a simple, theoretical discussion of how limb geometry influences the ability to step across hemispherical obstacles, and to confirm this geometry in animals who face relevant



conditions. The analysis was not performed with a specific robot in mind and should generalize among legged platforms that have two coplanar joints. This includes robots with dog-like legs in figure 1, and crab-like legs in figure 1. The analysis is for a single leg that works with other similar legs to form a gait. We envision a gait in which multiple stance legs work together to create opposing forces for stabilization, which can be accomplished by moving either one leg at a time for stability or moving more legs in phase, for example in an alternating tripod gait. This work does not address the control or trajectory planning for the limbs to find the valleys, but other work suggests that this is possible either passively [27, 38] or with vision [8, 39]. Instead, we are answering the question: how does the ratio of distal to proximal length of a two-jointed leg influence the ability to reach over hemispherical obstacles of varying sizes and produce

sufficient traction for force closure and successful walking?

First, we address this question using theoretical modeling. We idealize the environment as adjacent hemispherical rocks with valleys between them, which is a generalization that can be related to smooth river rocks, ribbed plant surfaces, cable-wrapped objects, or a set of parallel pipes or logs. We analyze the performance of stepping on this terrain using a leg with two parallel joints (a ‘hip’ and a ‘knee’), figure 2 and varying segment lengths. In figure 3, we summarize the result of our approach. Second, we directly measure the limb anatomy of two intertidal, sideways-walking crab species, comparing how limb length and relative segment lengths vary with species, body size, and leg number.



Our findings are applicable to both crab-like robots [27, 38, 40] and planar quadrupeds, e.g. dog-like robots [23, 41] in figure 1 and a robot with abstracted insect-like legs [42, 43]. In addition to inspiring robotic leg design, our findings inform our understanding of walking in any animal with limbs that can be approximated as two segments and that are restricted to a planar motion (e.g. horses, some spiders, and humans with rigid-ankle prostheses).

2. Methods

2.1. Modeling the workspace

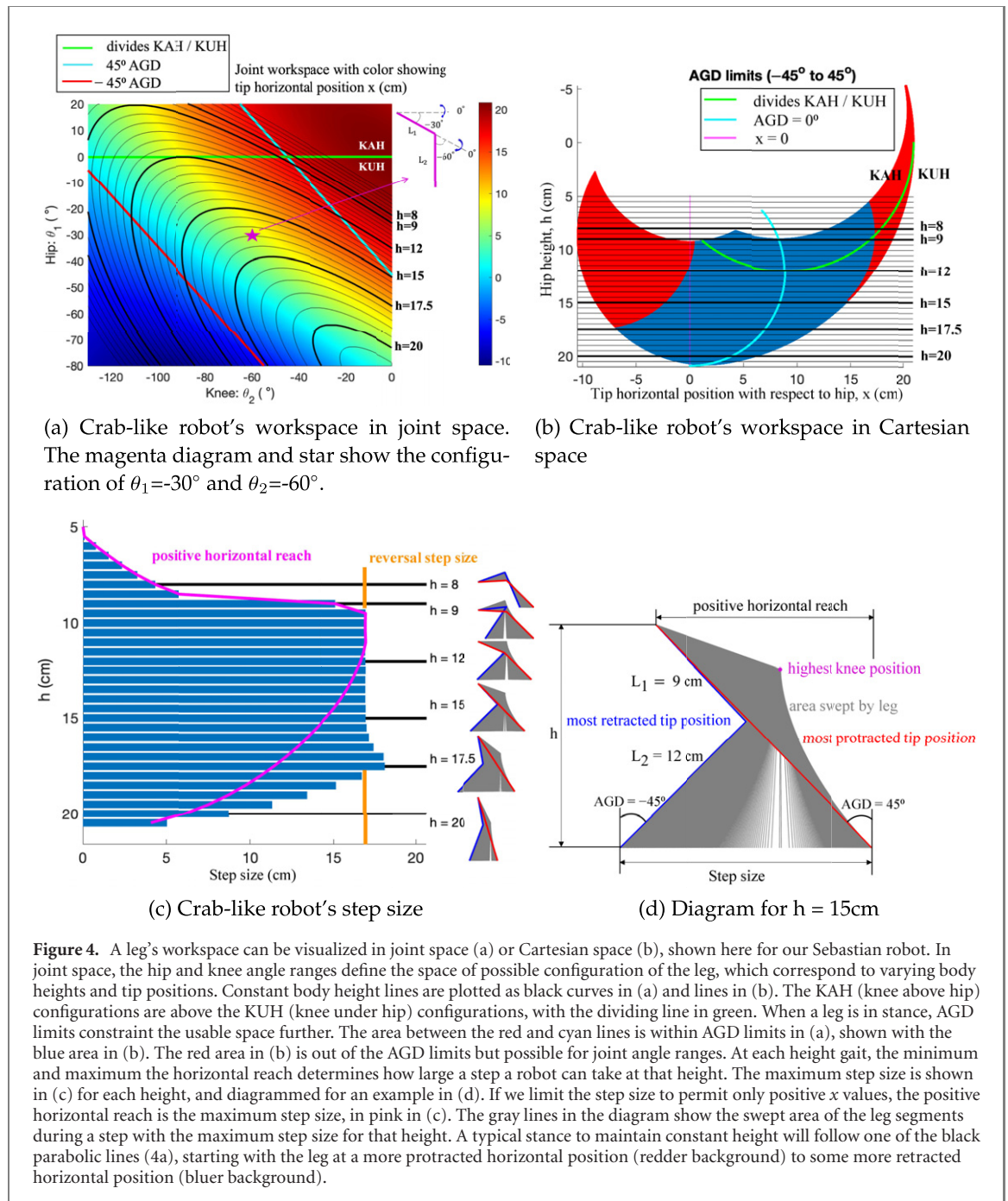
We assume a jointed leg with two co-planar joints (i.e., their axes of rotation are parallel to each other). The proximal joint can be thought of as the 'hip,' θ_1 , and the distal joint works as the 'knee,' θ_2 (figure 2). While articulated animal legs can have seven or more links, with multiple degrees of freedom (DOF) at each joint, robot efficiency and robustness typically depends on using as few joints as possible [9, 44–46]. Therefore, a common configuration [4, 8, 9, 45, 47–49] is to include two co-planar joints distal to an additional 'shoulder' joint whose axis of rotation is vertical. In forward walking, rotation of the shoulder around this vertical axis contributes most towards propulsion, rotating the entire leg, which undergoes small adjustments to keep body height level and raise the feet at onset of swing. Sideways walking primarily involves flexion and extension of the leg at the hip and knee joints, with small rotations around the vertical axis of the hip only for steering. We have previously shown that sideways walking is more efficient and enables

longer step sizes [27]. Thus here, to cross rocks, we will use sideways walking to take advantage of the way the two co-planar joints maximize the horizontal reach of robots, figure 4(c), to cross rocks.

The joints themselves have joint angle limits. While wheel-legs can continuously rotate in 360° [7, 24, 50–58] and other robots can invert legs to operate upside-down [7, 41, 49, 59], many robots, like the animals they are designed to mimic, have joint limits that influence the workspace of the legs. Rotations beyond 180° can cause leg segments to interfere. Our robot's servos, Savox SW-2210 TG, have a range of 130° . With a rectangular joint space of $\theta_1 (-80^\circ, 20^\circ)$ and $\theta_2 (-130^\circ, 0^\circ)$, figure 4(a), which is representative of our robot, the dactyl can reach the modified crescent space of figure 4(b).

Furthermore, the angle of the dactyl with respect to the ground AGD is a critical constraint determined by the joint angles, figure 2. We follow the convention of $AGD = 0$ [27] when a distal leg segment is vertical (perpendicular to the ground). A positive AGD indicates a dactyl pointing out away from the body, and a negative AGD indicates a dactyl pointing medially towards the body (figure 4(c)) [27]. In many robots, the end-effector will be designed to operate under a certain range of AGD for stability, which further limits workspace, section 3.1, even on flat ground. The effects of uneven ground on AGD are expanded in section 2.2.

Finally, ideal gaits maintain a desired constant body height, h in figure 2. A constant height is valuable for stabilizing any instruments on the body of a robot and direct teleoperation [39, 60]. Maintaining



constant height is one of the advantages of having a hip and a knee, unlike, for example, a spoke-like leg [52, 54, 61, 62]. The gaits to keep the constant body height are applied in [27, 38, 40].

2.2. Interactions between valleys and dactyl tips determine R/r and L_2

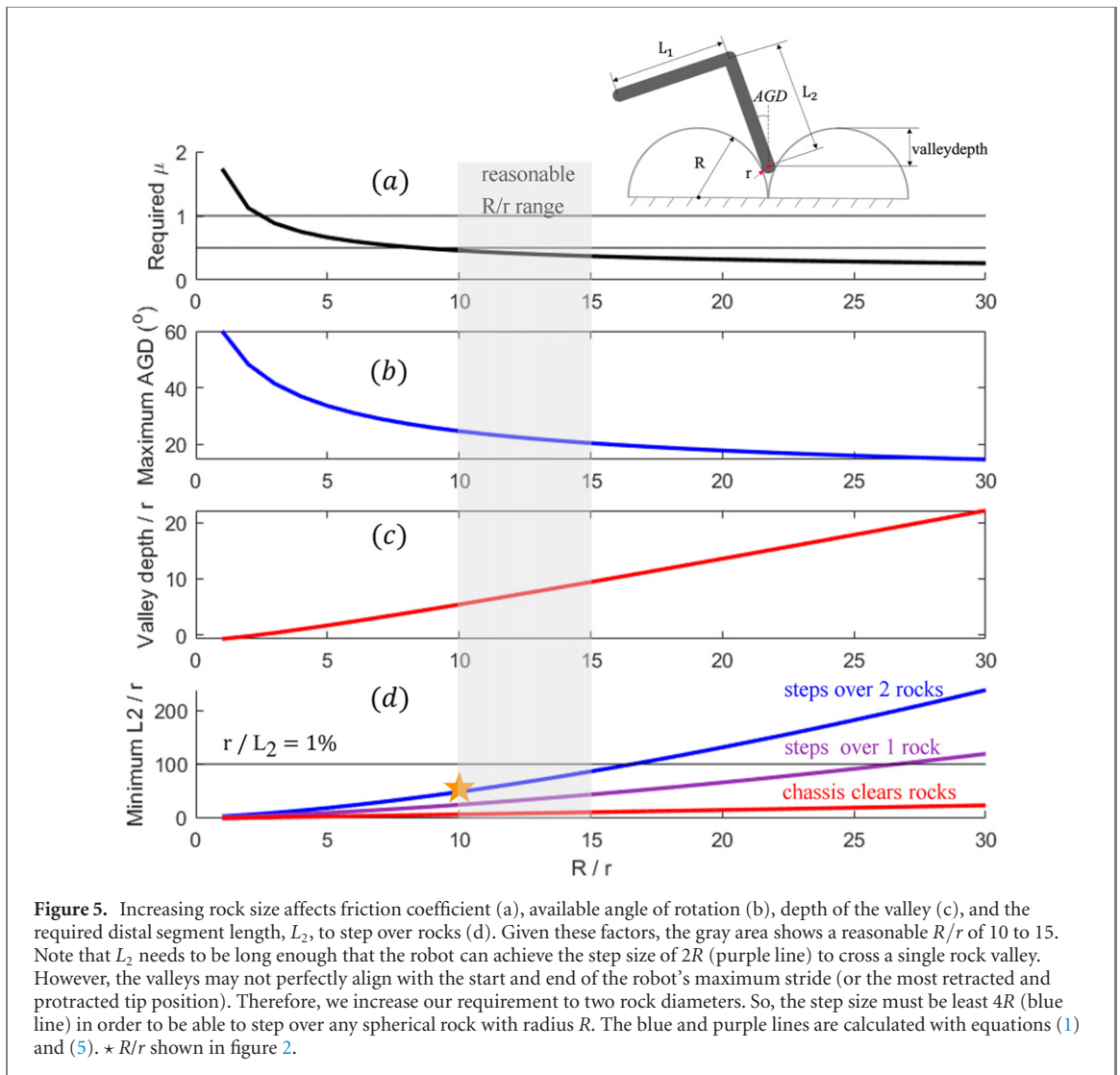
The 'valley' created between two hemispheric rigid 'rock' objects creates additional constraints, which can be best considered by R/r (the ratio of rock radius, R , to foot tip radius, r), figure 2. The smaller the tip, the deeper it can get into the valley. The depth of the valley is found by considering an isosceles triangle with two side lengths $(R + r)$ and one side length $2R$, figure 2(c). Thus, the angle β , figure 2, is 1;

$$\beta = \arccos\left(\frac{R}{R+r}\right) \tag{1}$$

and thus valley depth is

$$\text{valley depth} = R - (R+r) \sin \beta. \tag{2}$$

The deeper the dactyl can go into the valley, the better the legs can grasp rocks. With a sharp tip, and a very deep valley, the surface normal to the contact approaches horizontal. In this case, friction forces will be able to counter vertical forces (as long as the legs are strong enough to apply sufficient normal forces). In grasping, this is a force closure grasp, since any disturbance force can be resisted by increasing normal



force. In contrast, if the tip can only shallowly enter valleys, increasing inward forces only pushes the robot away from the ground. Assuming Coulomb friction, for every rock with radius R and a dactyl tip with radius r , there is a minimum friction coefficient, μ , figure A1, required to be able to grasp the ground with force closure

$$\mu = \frac{1}{\tan \frac{\alpha}{2}}, \quad (3)$$

where α is shown in figure 2(c), and determined by the same triangle as in equation (1) to be

$$\frac{\alpha}{2} = \arcsin\left(\frac{R}{R+r}\right). \quad (4)$$

Note that $\alpha/2 = 90^\circ$ for an infinitely small tip. Therefore the R/r determines μ , figure 5(a).

However, deeper valleys limit the AGD, reducing the step-size. Specifically, the angle β limits the AGD. Beyond β , the dactyl begins to rotate out of the valley, and the expected valley depth will not be achieved for grasping. With a limited AGD due to relatively large rocks and small tip, being able to step from one rock valley becomes a limitation.

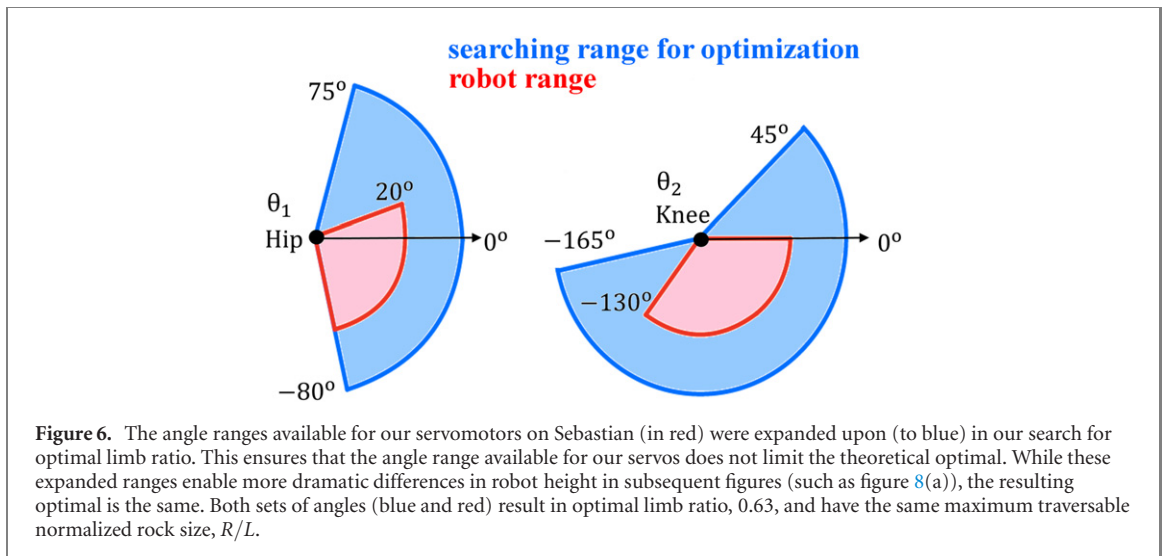
In this way, the ratio of R/r will have upper and lower bounds. Too low will require unrealistic friction coefficients (beyond the reasonable friction coefficients of uneven terrains, [63, 64]) for force closure. Too high will require the legs to be unrealistically long and spindly in order to step from valley to valley between rocks.

One final consideration is that the robot height also needs to be above the valley depth. If the legs are affixed to the bottom of the robot (i.e. no additional clearance for the chassis is needed), the valley depth limitation is shown in figure 5 with equation (2). Note that this is typically less restrictive than the requirement to step between rocks.

2.3. Optimizing limb ratio for sufficient positive horizontal reach

After determining the tip radius (r) and distal segment length (L_2), the remaining leg parameter to consider is L_1 .

The primary advantage of increasing L_1 is that the height of the robot can be varied over a larger range and still achieve the required step size to cross the rock diameters. A longer L_1 provides a more



sprawled posture when it is desired, for example, for interacting with the ground or keeping a low profile in waves or climbing. Therefore, at a desired height, increasing L_1 increases the horizontal distance of the dactyl from the body. This increases the torque requirements at the hip and has other trade-offs with more sprawled posture [65]. Note that at each height, a slightly different range of angles will be required, but generally the width of the range is about the same, figure B2.

Allowing the dactyl tip to cross underneath the body incurs risks. First, when the support polygon is smaller than the body, stability is no longer guaranteed for uneven body weight distributions. Second, if the body is narrow, the workspace of the legs on either side of the body can overlap, potentially entangling legs. Furthermore, depending on the swing trajectory, the dactyl can interfere with the body.

Thus, we limit the workspace to the positive side of the magenta line in figures 4(b) and (c) (magenta line). With this final limitation, the optimal L_1 is determined by the limb ratio that can cross the maximum rock size (and the largest traversable rock size range). Across all possible body heights, we determine the maximum step size possible, normalized by rock diameter for different limb ratios. As the limb ratio approaches an optimal, larger rocks are traversable. The angles' range chosen for searching optimization is shown in figure 6. This searching range aims to show the optimal limb ratio is generalized for different servos and other robots so that the method introduced could be extended to other's research. Also, this searching range demonstrates different heights most clearly as shown in figure 8(a). In addition, when using our robot range (red in figure 6, which aligns with that of figures 4(a) and (b)) for optimization, the optimal limb ratio and maximum traversable rock size remain the same.

2.4. Biological crab data collection

Crab limbs consist of seven exoskeleton segments, with three functionally fused: coxae (Co), basi-ischio-merus (BIM), carpus (C), propus (P), and dactyl (D) [66]. Flexion and extension of the limb joints in the coronal plane occurs mostly at the Co-BIM and M-C joints, figure 2. While the P-D joint exhibits a wide range of motion, the relatively short length of the dactyl causes movement at this joint to not dramatically influence overall leg length or dactyl placement.

To investigate the leg anatomy of crab walking limbs, we collected lined shore crabs (*Pachygrapsus crassipes*) and purple shore crabs (*Hemigrapsus nudus*) from La Jolla, CA and Tillamook Bay, OR respectively (ODFW Scientific Taking Permit 25817). The choice of crab species (*Hemigrapsus nudus* and *Pachygrapsus crassipes*) centers around three aspects. First, the crabs walk primarily sideways, inducing the walking limbs to move in a mostly planar motion relevant to our theoretical analysis. Second, these species are 'intertidal' meaning that they navigate extensively over rocky, uneven substrates (and on granular sand). Third, these species are accessible for collection and maintenance under laboratory conditions. The two species are similar in size with some overlapping range.

Crabs were sacrificed via cold anesthesia, weighed (± 0.001 g), and briefly dipped in ethanol for disinfection. The eight pereopods from each crab were removed above the thoraco-coxopodite joint using forceps and labeled as legs 2–5 (on the left and right). Many crabs had missing legs. In total we analyzed 22 crabs and 172 legs for *H. nudus* and 17 crabs and 78 legs for *P. crassipes*. For each leg, the basi-ischio-merus (BIM), carpus (C), propus (P), and dactyl (D) segment lengths were measured using calipers (Adoric B08DLQP1T6) from mid-joint to mid-joint,

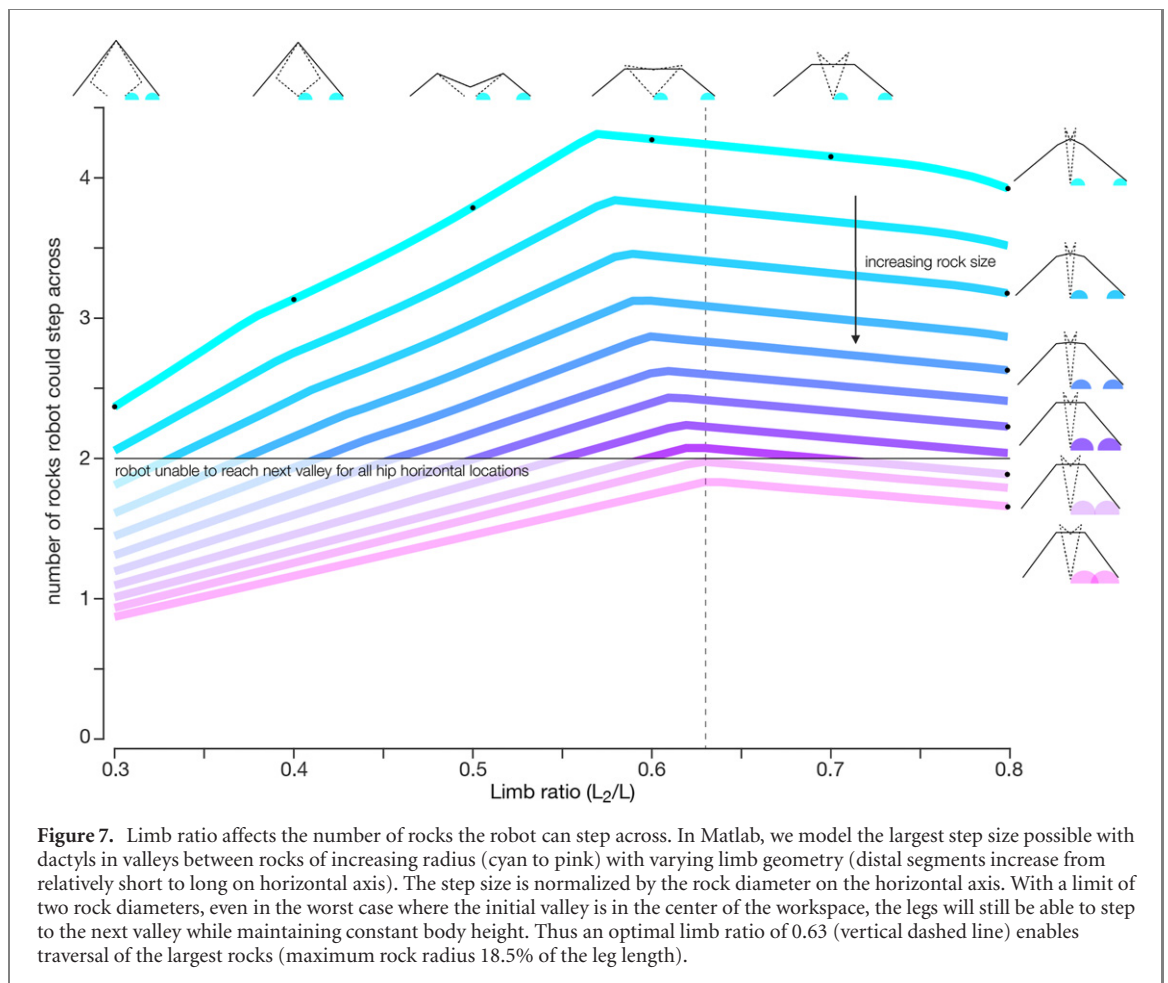


figure 2. For nine *H. nudus* specimens, the Co-BIM, M-C, and P-D joints of each leg were photographed at maximum extension and flexion for the angular range of motion relative to the long-axis of the proximal segment (ImageJ, [67]).

The total limb length and limb ratio of each pereopod was compared using linear mixed effect models (LMER package in R). The limb length was compared for both species (LegLength LegNumber + Species + Species|ID), whereas limb ratio was analyzed just for *H. nudus* due to a limited size range in *P. crassipes* (LimbRatio CarapaceWidth + LegNum + Sex|ID). For all LME models, data normality was confirmed using quartile–quartile, histogram, and residual plots. Significance was determined using ANOVAs comparing the full and a reduced model. For limb ratio in *H. nudus*, sex was found to be insignificant and was removed as a factor for the final analyses (LimbRatio CarapaceWidth + LegNum + 1|ID).

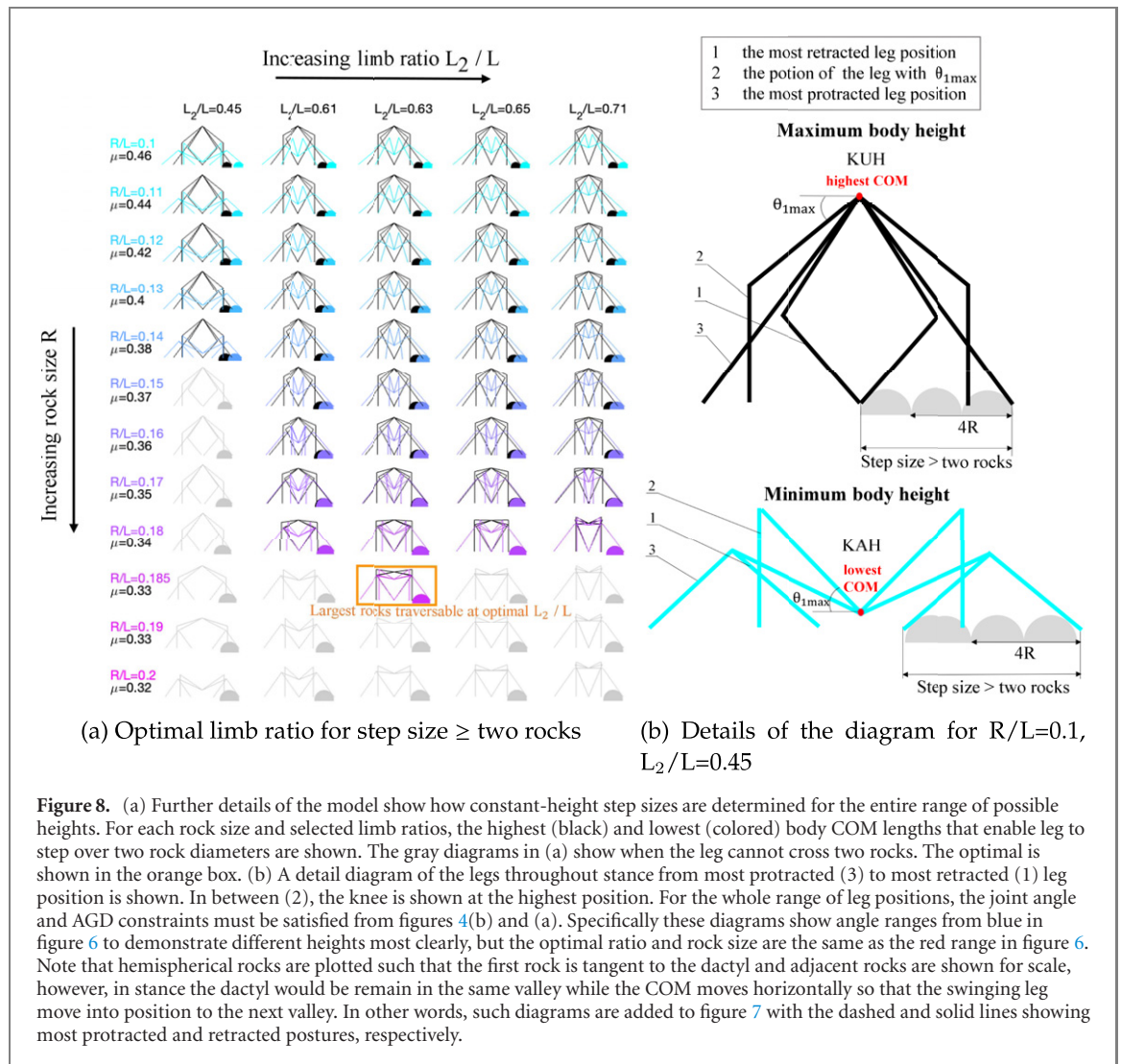
3. Robotics results

3.1. Workspace and step size at height

Geometric limits determine the leg's workspace, which in turn, limits the maximum step size especially when body is close to the ground. The ground angle

AGD limits create a diagonal band of usable joint angles in figure 4. The maximum step size can be found by taking the difference between the maximum and minimum horizontal points at a particular height, figure 4(c). To take a constant-height step, the legs may pass through qualitatively different configurations, for example from KUH to KAH and back to KUH. If the knee is under the hip KUH, figure 8(b) (i), the posture is more upright like a quadruped or human walking. When the knee is above the hip KAH, figure 8(b) (ii), the posture is sprawled like an archetypal crab. When the body is too close to the ground (height of the hip less than 9 cm), geometric constraints prevent the legs from becoming KUH, and therefore the leg cannot reach both positive and negative AGD limits without changing height. In other words, when the workspace separates into non-contiguous lobes, the dactyl is not fully reversible. Thus, although the dactyl placement can allow hip heights as low as 5 cm off the ground, the step size is greatly reduced when the body is low to the ground.

At a large range of intermediate heights, the maximum step size is achieved by proceeding from the positive AGD limit to the negative AGD limit. In other words, the L_2 link reverses the direction such that the starting and ending angles of the L_1 link are the same (e.g. the diagrams for $h = 12$ cm at the right of figure 4(c)). So the reversal step size (figure 4(c)) can



be described in equation (5) based on the diagram in figure 4(d)

$$\text{reversal step size} = 2L_2 \sin(\text{AGD}). \quad (5)$$

Note that at higher body heights, a slightly longer maximum step size occurs when the start and end positions of the L_1 are different, as diagrammed for height of 17.5 cm in figure 4(c). When the robot is too high (the bottom of the figures 4(b) and (c)), the step sizes can be limited by the joint angle limits, such as minimum θ_1 , figure 4(a).

However, while there are advantages and disadvantages to a sprawled posture (along the positive x -axis), folding the legs under the body (left of the magenta vertical line in figure 4(b)) is less useful. The more extended the dactyl in the positive x direction (sprawled posture), the larger the support polygon and thus the higher the stability. The biggest trade-off is that the transverse loads on the legs and joints are increased. For crabs in water, the disadvantageous loading may be mitigated by neutral buoyancy and sprawling is likely to help resist hydrodynamic forces [68]. Using both sprawled postures (for stability in waves and climbing) and tall postures

(to traverse high obstacles or deep valleys) could make sense. However, while the dactyl can reach negative x -values (medial beneath the hip), these positions decrease robot stability, increase required actuation torques, limit obstacle height clearance, and can create leg interference problems.

Thus, if we consider only the positive part of the workspace, the step size is limited to the maximum positive position of the dactyl (the positive horizontal reach in figure 4). Interestingly, the largest possible step including both positive and negative dactyl positions is in the KUH region, while the maximum step size is in the KAH combined KUH region. In other words, for walking while keeping the legs comfortably forward a KUH posture is best, but if a larger step is needed a lower crab-like KAH posture could be adopted.

3.2. Rock to tip radius range

The friction coefficient, μ , provides a lower bound on the ratio of the rock radius to dactyl tip radius R/r . Larger friction coefficients become inconsistent with Coulomb friction. According to equations (3) and (4), $R/r < 10$ could require a friction coefficient $\mu \geq 0.5$,

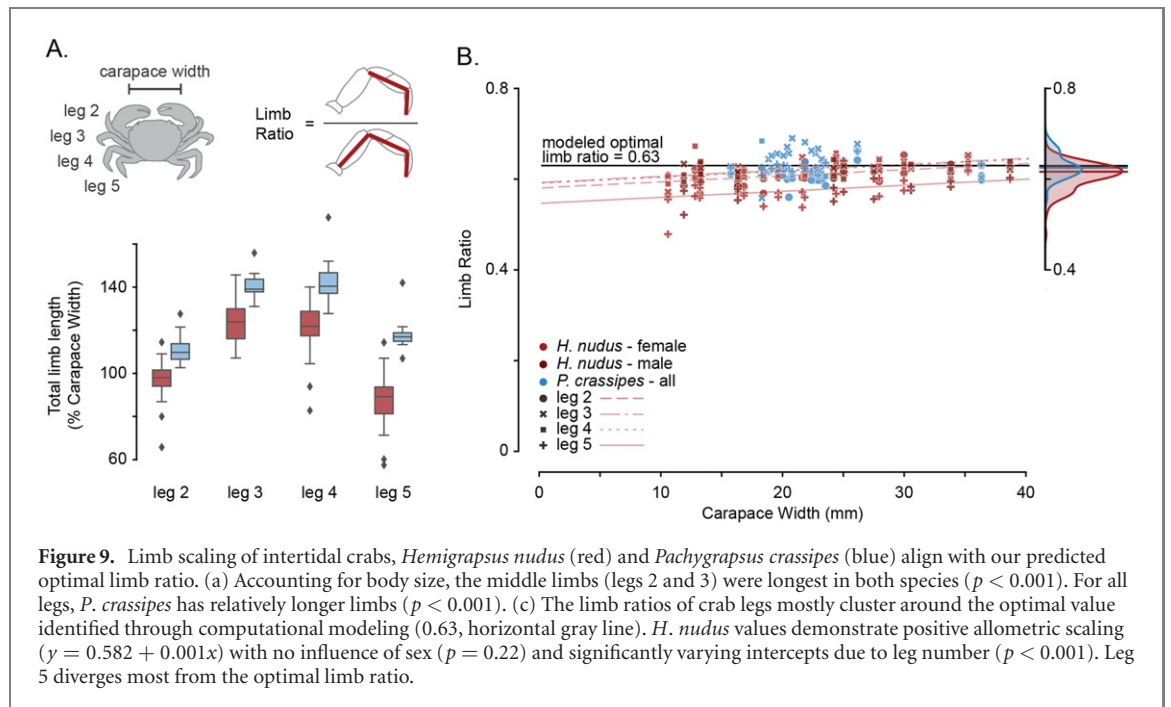


figure 5(a), which seems unreasonable for smooth, potentially wet natural surfaces [63, 64].

However, step size creates an upper bound on the rock to dactyl radius ratio R/r . Increasing R/r constrains AGD, figure 5(b), and increases valley depth figure 5(c). As a result the minimum L_2 to step between valleys increases, figure 5(d). If L_2/r is too high, indicating a long dactyl with small diameter, the leg will be susceptible to bending and material failures. Thus, we set an upper bound of when $R/r = 15$ such that the minimum r/L_2 is less than 1%, figure 5(d).

3.3. Optimal robot limb ratio from simulations

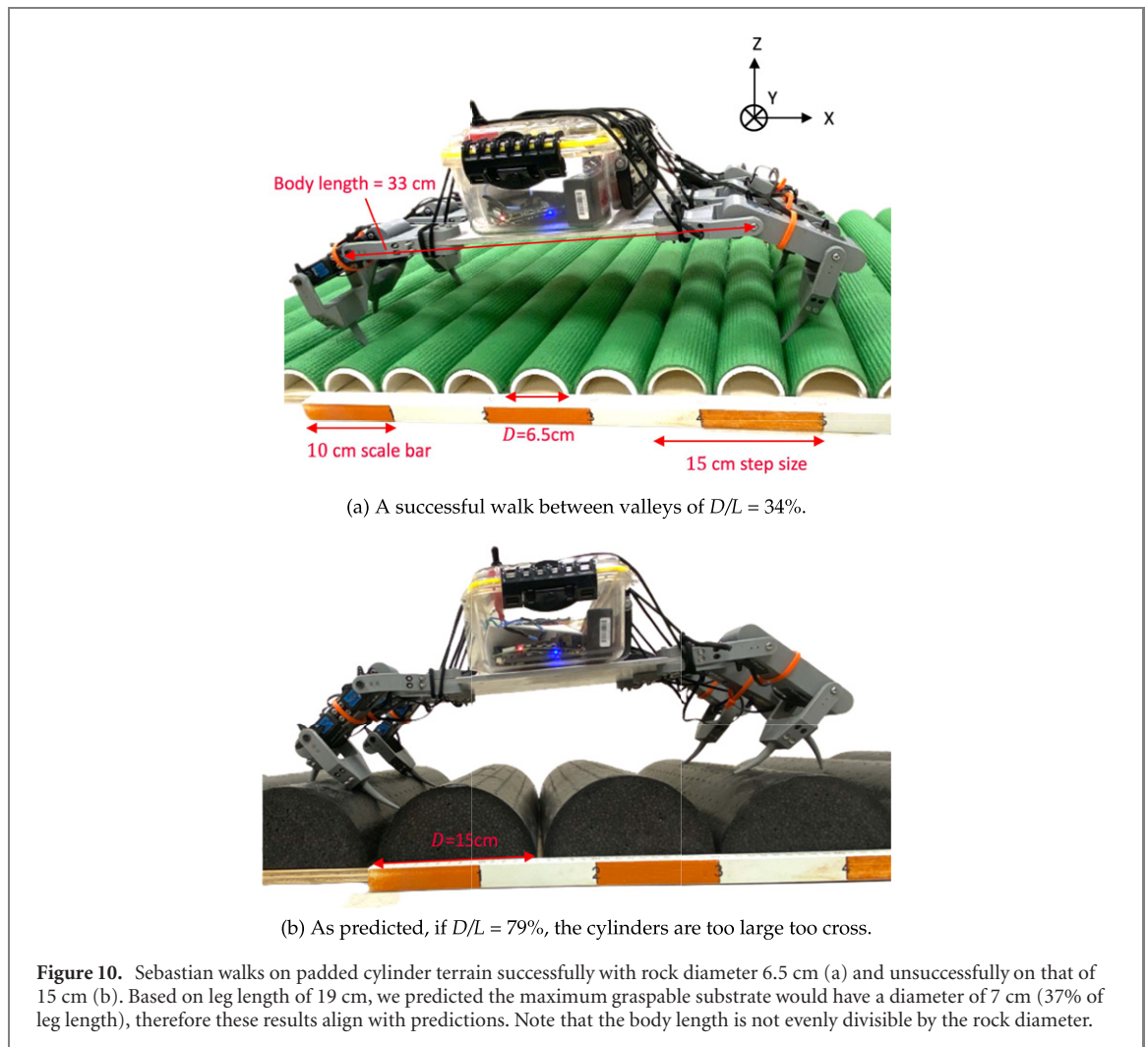
We ran simulations for a given toe tip width while varying hip height, rock size, and the relative lengths of the leg segments. The output of these simulations calculated the most protracted and retracted positions of the limb while successfully placed in a valley. The horizontal distance between these foot locations was normalized by rock size, representing the maximum distance the leg could step in terms of rock diameters. All simulations used a tip radius of 1% of the total leg length L ($L = L_1 + L_2$). The range of motion of each joint was constrained as shown in figure 6. While some animals have been observed to lower their body to extend their reach for a desirable foothold [69], our goal is to create a gait that keeps the body (and therefore hip) height constant, which increases body stability and simplifies limb control.

To maintain mobility along a substrate of parallel hemispherical rocks, a leg must be able to step more than two rock diameters ($4R$). Even if the body chassis length is not an even multiple of rock diameters, a step size of two rock diameters

guarantees that the legs will be able to step to the next valley regardless of where the initial valley is in the workspace. As a counterexample, imagine a leg with a maximum step length of one rock diameter. If the initial valley is directly under the hip, the leg can step to the next valley foothold one rock distance protracted away from the body. However, if the current foothold is slightly offset away from the body, it cannot make the subsequent step. A step length of two rock diameters ensures that the leg can reach any next valley.

For each rock size (which we normalize to leg length), we identified an optimal limb ratio, L_2/L , that maximized step length (the vertical peak of each line in figure 7). Relatively small rocks permitted step lengths of more than two rocks ($4R$) for all leg geometries. However, larger relative rocks constrained the number of rocks that could be stepped over to fewer than two. Using this threshold, the largest hemispherical rocks able to be transversed in a field of parallel rocks had a radius of 18.5% of the total leg length. Rocks close to this cut-off required a ratio of the limb segments of 0.63, meaning the distal portion of the limb comprises 63% of the total limb length, $L_2/(L_1 + L_2)$ 8a.

Note that these data assume angle ranges defined in the blue in figure 6 for broadest optimization. However, the limb ratio is not particularly sensitive to angle range, and simulations using the red range in figure 6 also identified an optimal ratio of 0.63. Presenting the data using the wider blue range emphasizes the differences in minimum and maximum hip height, for example in figure 8(b), and so is better for plotting and shows our optimal can be relevant for animals with greater range of motion.



4. Limb ratio in the walking legs of crabs

Analysis of 250 walking legs from two species of intertidal crabs revealed length variation between species and among limbs, figure 9. When normalized for crab body size, the middle limbs (legs 3–4) were at least 25% longer than the most anterior and posterior limbs (legs 2 and 5) ($p < 0.001$), figure 9(A). This pattern represents a new observation within crabs. While many studies focus on the scaling of the chelae (claws), only a few discuss the pereopods (walking legs). Pereopod analysis often relies on only one limb ([66] or averages across all limbs [70]. To the best of our knowledge, only one study has compared limb lengths among legs in crustaceans, finding modest (5%) variation among limbs for a side-walking *Carcinus* crab [71]. In addition to limb length, the geometry of the pereopods varied with leg number. In *H. nudus* crabs, the most posterior leg had a relatively longer proximal portion ($p < 0.001$). Together, these findings suggest a possible functional specialization within the ‘walking’ legs. Several species of aquatic crabs possess flattened posterior pereopods, which are used as paddles during swimming [72]. The among-limb variation observed here in intertidal crabs could

result from evolutionary constraints related to these swimming posterior limbs or indicate a selective shift associated with limb use. Intertidal crabs, like *H. nudus* often hide under rocks or in crevices. The posterior legs could have evolved to best buttress the crab against rocks, especially when exposed to strong waves and currents.

Despite modest variation among limbs, the geometry of intertidal crab walking legs aligns closely with the optimal value calculated from computational models. The median limb ratios were 0.612 and 0.624 for *H. nudus* and *P. crassipes* respectively, figure 9(B), almost exactly aligned with the optimal 0.63 value found using simple computational modeling of a two-segment limb stepping over hemispherical obstacles.

5. Application of the optimal limb ratio in a hexapod robot

To validate the relevance of this paper’s findings for legged robots (like those in figure 1), we tested a hexapod robot, ‘Sebastian’, with double-segmented limbs walking over half-cylindrical pipes (figure 10 (a)). The pipes represented a rock radius of 17% of the total leg length, which is slightly smaller

than the maximum rock size calculated in the simulations above. We used a simple open loop control with step size 2.3 times the rock diameter and a limb ratio of 0.627. Additional hardware and parameters of Sebastian are listed in section appendix B. Videos of the robot walking are available at <https://drive.google.com/drive/folders/1BgKlBzgspeFhoJm-KjXrCURIqYDr2JoF>. Note, because the robot body length is 5.1 times the rock diameter, the front and rear legs interacted differently with the substrate, reinforcing the importance of a maximum step size greater than two rock diameters. While the maximum step size was 15 cm on flat ground, the robot was unable to walk in valleys of rocks at that diameter, as predicted by our analysis.

6. Conclusions and discussion

For two-jointed legs, which are common to many types of robots, as shown in figure 1, the essential contribution of this paper is the discovery of an optimal limb ratio for stepping between valleys created by idealized rocks, figure 5, and that this same optimal ratio is similar to the corresponding ratio in intertidal crabs such as *Hemigrapsus nudus* and *Pachygrapsus crassipes*. An optimal limb ratio L_2/L of 0.63 ensures that a leg with the tip size of 1% of the total leg length can step across at least two rocks. The resulting prediction is that the largest sequential rocks that the robot can walk across have a radius that is 18.5% of the total leg length, or a diameter that is 37% of the total leg length. We also demonstrate that the distal portion of a limb should have a thickness (R/r) that ranges from 10–15 to resist material failures while producing a reasonable friction coefficient when navigating across idealized adjacent hemispheric rocks.

We present here a first analysis using the idealized case of half cylindrical obstacles. While future work could extend into other combinations of rock diameters and shapes, vary hip height while stepping, or incorporate joints with more than one degree of freedom, our analysis can inform initial robotic leg designs. These designs can be scaled for a desired nominal environment or to optimize behavior. We demonstrate the benefit of these design insights using a hexapod robot (figure 10). Our findings predict that with a limb ratio of 0.63, this robot should be able to traverse rocks with a 7 cm diameter. Using a fixed step length of 15 cm open loop gait, the robot was able to walk across padded cylinders with 6.5 cm diameter. In trials with larger half cylinders, the legs of the robot rotate out of the valleys before completing the step.

Although the robotic validation presented in this study included legs that curve and taper at the end (mimicking a crab limb's dactyl), our findings also apply to legged robots that have an almost straight leg and nearly cylindrical geometry, such as

ANYmal and BigDog [9, 44]. The advantage of the curved dactyl is that it can increase the contact area (and therefore friction) with a hemispherical rock or hook into an overhanging asperity to increase the downward vertical force (clinging to the ground). Future work could investigate the optimal curvature of a dactyl when walking over hemispherical or variably-shaped obstacles.

This study focuses on a single limb, but does not address the interactions among multiple limbs or incorporate a body. Future work that develops gaits and incorporates sensing could optimize walking efficiency and enable behavioral versatility. Coordination of the limbs could increase walking speed (such as using an alternating tripod gait) or prioritize stability (stepping with one leg at a time). The legs of crabs also vary in length, with the middle legs longest. Incorporating multiple limbs and developing walking gaits may reveal how leg length variation influences walking over obstacles, especially under conditions where the obstacles vary in size. Adding a vision system that estimates upcoming rock size could enable real-time control of step length and leg motion. Tactile sensing at the leg tip could inform the precise placement of the feet in valleys before initiating inward forces. Gait optimization and sensing may also enable multi-modal movement, combining walking over uneven terrain with climbing [24].

The rocky terrain that intertidal crabs call home is highly variable, both spatially and temporally. Plus, these rocks serve as more than obstacles for walking, providing hiding crevices from predators and shelter from incoming waves. However, if the walking limbs of crabs evolved to effectively step across rocks, we would predict the rocks to have a diameter of less than roughly half the carapace width. We might observe this adaptation as smaller crabs preferring areas with smaller rocks, or as smaller crabs demonstrating higher leg injury rates and predation rates among larger rocks. Future work that measures limb geometry broadly across crabs could associate the anatomy of the walking limbs to habitat type, comparing closely-related species that live primarily on sand with those on rocky terrain. These investigations may also further explore the influence of variable leg length along the body. The most posterior limbs are specialized for swimming in pelagic crabs and can be observed buttressing intertidal crabs as they often stand backed against a rock. Additionally, recording crabs walking over artificial, hemispherical obstacles could quantify how the limbs interact with the substrate valleys, associate obstacle size with walking speed, and explore the implications of leg regrowth after autonomy.

The fact that the optimal limb ratio predicted by a simple two-segmented leg model is similar to that found in crab limbs suggests that the kinematics

induced by this limb geometry are relevant across different actuation mechanisms. Similar patterns in limb anatomy may appear more broadly among animals, informing the interpretation of limb function in both extant and extinct species. The findings of this paper provide an accessible set of limb design principles that can be applied for walking robots or leg prostheses tasked with moving over uneven terrain.

Acknowledgments

This research was partially funded by the Office of Naval Research under a Young Investigator Award (TTP19-0033) to Kathryn A Daltorio, by the Strategic Environmental Research and Development Program (SERDP) SEED Grant #MR19-1369 to Kathryn A Daltorio, and by a Research Start-up Grant from the M J Murdock Charitable Trust to Glenna T Clifton. The authors would like to thank Nathan Carmichael for drawing rendered robot legs and references. The authors would like to acknowledge the anonymous reviewers whose valuable comments have improved this paper.

Data availability statement

The data that support the findings of this study are openly available at the following URL/DOI: <https://drive.google.com/drive/folders/1BgKlBzgsPEFhoJm-KjXrCURIqYDr2JoF?usp=sharing>.

Appendix A. The free body diagram for force closure

Based on the free body diagram, figure A1, when the robot anchors on the obstacle,

$$f \cos(\beta) = N \sin(\beta) \quad (\text{A.1})$$

$$f = \mu N \quad (\text{A.2})$$

$$\beta = 90^\circ - \alpha/2, \quad (\text{A.3})$$

where f is the friction force and N is the normal force. When equations (A.1), (A.3) and (A.2) are combined, the minimum μ is 3.

Appendix B. Sebastian hardware and parameters

Sebastian's leg design [27, 38] is loosely inspired by the biological crab species *Pachygrapsus crassipes*, which is a small shore crab that typically walks sideways. As in crabs, the legs end in pointed dactyls. However, while shore crabs are often 5 cm long, our robot is scaled up to 33 cm long to accommodate standard SAVOX SW-2210 motors (figure B1 and table B1). Also, the robot is currently a hexapod in order to have the minimum number of legs for an alternating tripod gait. Thus, there are 12 DOF (figure B1 and table B1). All of the leg pieces are 3D printed (MarkerGear M2, PLA, 100% infill). The chassis contains batteries and electronics for control and data collection. The robot uses a Raspberry Pi 4B powered by a PiSugar2 Pro as its on-board CPU, which communicates with a 12-pin PololuMaestro servo controller. A 7.4 V lithium polymer battery powers the motors. A basic gait is described in a companion paper [73] (figure B1 and table B1).

We estimate the coefficient of friction between the substrate and the dactyls to be between 0.4 and 0.5 based on [74, 75]. Here we have wrapped the substrate with the high friction surface (a PVC mat) and the dactyls have low friction (3D printed PLA). In practice the dactyls could also be coated with a high friction coating for walking on low friction surfaces such as smooth rocks.

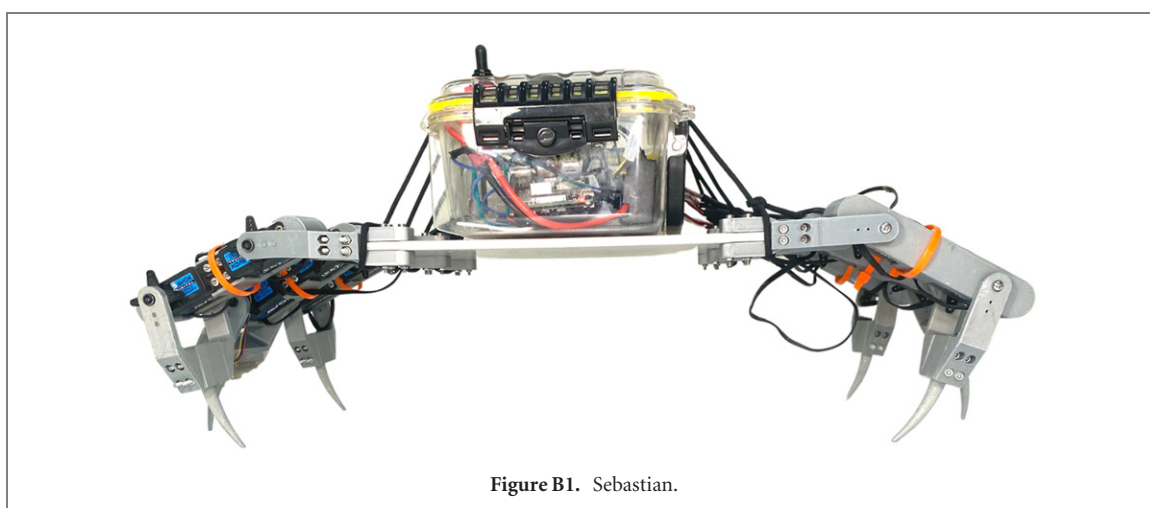
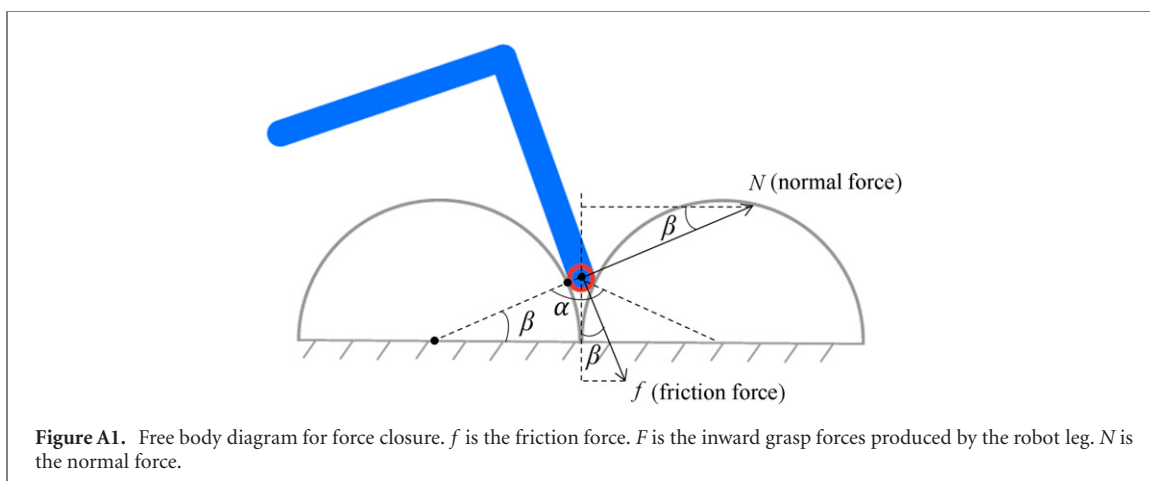
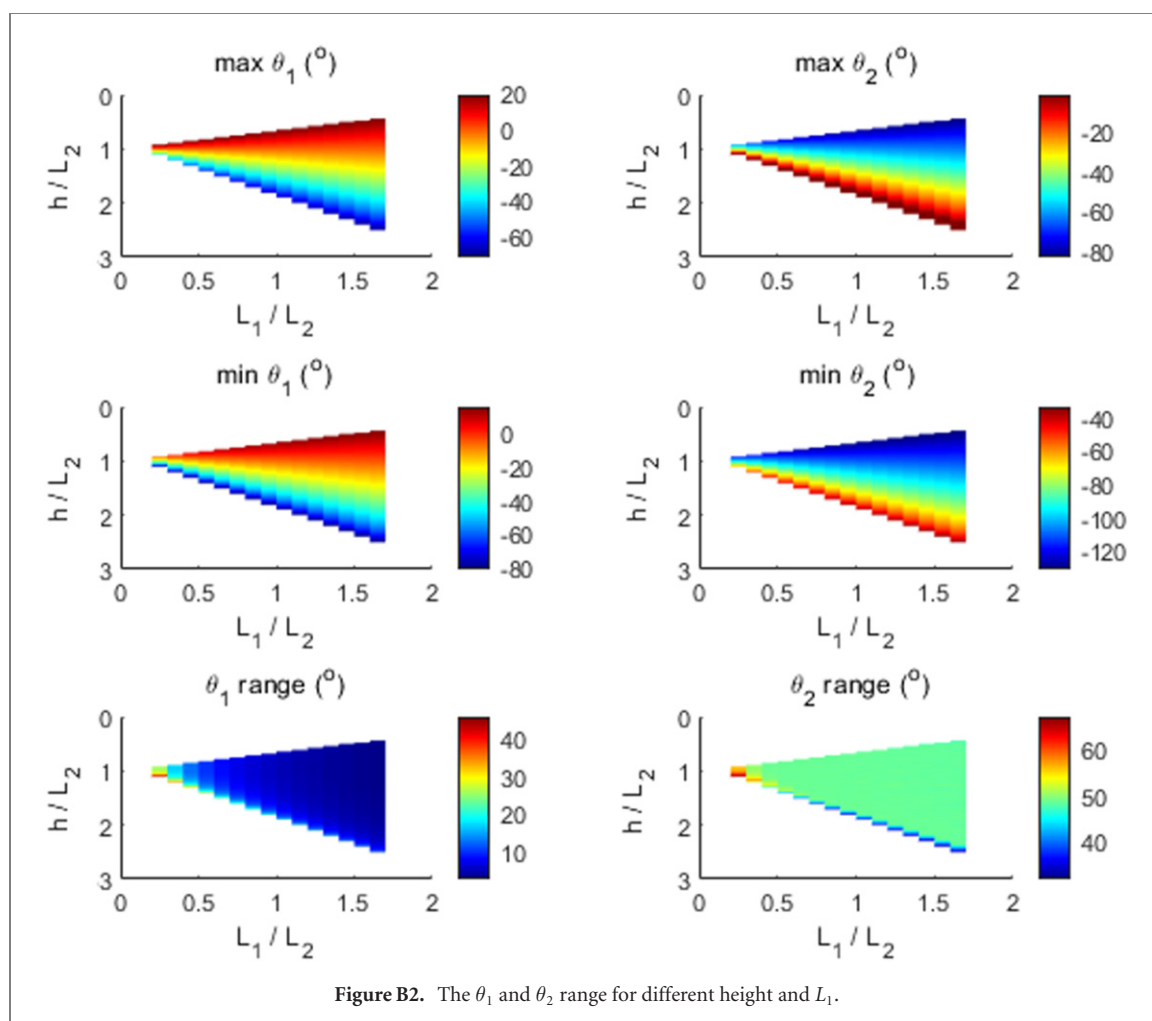


Table B1. Robot dimensions.

	Length (cm)	Weight (g)
Total robot	33 ^a	4327
Body	20 ^b	2248.6
1 Coxa (L_1)	5.4	71.6
1 Tibia (L_3 , 2 servos included)	7.5	218.5
1 Dactyl (L_4)	12.6	56.3

^aThe minimum length of Sebastian in the Y direction (figure 10(a)), when the robot is standing.

^bThe length of Sebastian in the X direction (figure 10(a)).



ORCID iDs

Yang Chen  <https://orcid.org/0000-0001-7380-5756>

Nicole M Graf  <https://orcid.org/0000-0001-9207-0441>

References

- [1] Zucker M, Bagnell J A, Atkeson C G and Kuffner J 2010 An optimization approach to rough terrain locomotion *2010 IEEE Int. Conf. Robotics and Automation* (Piscataway, NJ: IEEE) pp 3589–95
- [2] Boxerbaum A S, Oro J, Peterson G and Quinn R D 2008 The latest generation Whegs™ robot features a passive-compliant body joint *2008 IEEE/RSJ Int. Conf. Intelligent Robots and Systems* (Piscataway, NJ: IEEE) pp 1636–41
- [3] Morrey J M, Lambrecht B, Horchler A D, Ritzmann R E and Quinn R D 2003 Highly mobile and robust small quadruped robots *Proc. 2003 IEEE/RSJ Int. Conf. Intelligent Robots and Systems (IROS 2003)* (Cat. No. 03CH37453) vol 1 (Piscataway, NJ: IEEE) pp 82–7
- [4] Graf N M, Behr A M and Daltorio K A 2019 Crab-like hexapod feet for amphibious walking in sand and waves *Conf. Biomimetic and Biohybrid Systems* (Berlin: Springer) pp 158–70
- [5] Goldman D, Komsuoglu H and Koditschek D 2009 March of the sandbots *IEEE Spectr.* **46** 30–5
- [6] White J D S and Hubicki C 2020 Force-based control of bipedal balancing on dynamic terrain with the ‘tallahassee cassie’ robotic platform *2020 IEEE Int. Conf. Robotics and Automation (ICRA)* (Piscataway, NJ: IEEE) pp 6618–24
- [7] Full R 2000 Unlocking the secrets of animal locomotion retrieved from <https://berkeley.edu/news/media/releases/2002/09/rfull/robots.html>
- [8] Gehring C, Fankhauser P, Isler L, Diethelm R, Bachmann S, Potz M, Gerstenberg L and Hutter M 2021 Anymal in the field: solving industrial inspection of an offshore HVDC platform with a quadrupedal robot *Field and Service Robotics* (Berlin: Springer) pp 247–60
- [9] Fankhauser P and Hutter M 2018 Anymal: a unique quadruped robot conquering harsh environments *Res. Featur.* **126** 54–7
- [10] Lee J, Hwangbo J, Wellhausen L, Koltun V and Hutter M 2020 Learning quadrupedal locomotion over challenging terrain *Sci. Robot.* **5** eabc5986
- [11] Bretl T, Rock S and Latombe J C 2003 Motion planning for a three-limbed climbing robot in vertical natural terrain *2003 IEEE Int. Conf. Robotics and Automation (Cat. No. 03CH37422)* vol 3 (Piscataway, NJ: IEEE) pp 2946–53
- [12] Nagaoka K, Minote H, Maruya K, Shirai K Y, Yoshida T, Hakamada H, Sawada T and Kubota T 2018 Passive spine gripper for free-climbing robot in extreme terrain *IEEE Robot. Autom. Lett.* **3** 1765–70
- [13] Parness A, Neil A, Fuller C, Wiltsie N, Nash J and Kennedy B 2017 Lemur 3: a limbed climbing robot for extreme terrain mobility in space *2017 IEEE Int. Conf. Robotics and Automation (ICRA)* (Piscataway, NJ: IEEE) pp 5467–73
- [14] Tramsen H T, Heepe L, Homchanthanakul J, Wörgötter F, Gorb N S and Manoonpong P 2021 Getting grip in

- changing environments: the effect of friction anisotropy inversion on robot locomotion *Appl. Phys. A* **127** 389
- [15] Spenko M J, Haynes G C, Saunders J A, Cutkosky M R, Rizzi A A, Full R J and Koditschek D E 2008 Biologically inspired climbing with a hexapedal robot *J. Field Robot.* **25** 223–42
- [16] Wile G D, Daltorio K A, Diller E D, Palmer L R, Gorb S N, Ritzmann R E and Quinn R D 2008 Screenbot: walking inverted using distributed inward gripping 2008 *IEEE/RSJ Int. Conf. Intelligent Robots and Systems* (Piscataway, NJ: IEEE) pp 1513–8
- [17] Saunders A, Goldman D I, Full R J and Buehler M 2006 The rise climbing robot: body and leg design *Unmanned Systems Technology VIII* (Orlando (Kissimmee), Florida, United States 2006) vol 6230 p 623017
- [18] Wieber P-B, Tedrake R and Kuindersma S 2016 Modeling and control of legged robots *Springer Handbook of Robotics* (Berlin: Springer) pp 1203–34
- [19] Khorram M and Moosavian S A A 2017 Push recovery of a quadruped robot on challenging terrains *Robotica* **35** 1670–89
- [20] Espenschied K S, Quinn R D, Beer R D and Chiel H J 1996 Biologically based distributed control and local reflexes improve rough terrain locomotion in a hexapod robot *Robot. Autonom. Syst.* **18** 59–64
- [21] Ruotolo R, Roig S and Cutkosky M R 2019 Load-sharing in soft and spiny paws for a large climbing robot *IEEE Robot. Autom. Lett.* **4** 1439–46
- [22] Wang S, Jiang H and Cutkosky M R 2016 A palm for a rock climbing robot based on dense arrays of micro-spines 2016 *IEEE/RSJ Int. Conf. Intelligent Robots and Systems (IROS)* (Piscataway, NJ: IEEE) pp 52–9
- [23] Ackerman E 2021 *Q & A: Ghost Robotics CEO on Armed Robots for the US Military* <https://spectrum.ieee.org/ghost-robotics-armed-military-robots> 18 October 2021
- [24] Saranli U, Buehler M and Koditschek D E 2001 Rhex: a simple and highly mobile hexapod robot *Int. J. Robot. Res.* **20** 616–31
- [25] Daltorio K A, Wei T E, Gorb S N, Ritzmann R E and Quinn R D 2007 Passive foot design and contact area analysis for climbing mini-Whlegs *Proc. 2007 IEEE Int. Conf. Robotics and Automation* (Piscataway, NJ: IEEE) pp 1274–9
- [26] Daltorio K A, Wei T E, Horschler A D, Southard L, Wile G D, Quinn R D, Gorb S N and Ritzmann R E 2009 Mini-Whlegs tm climbs steep surfaces using insect-inspired attachment mechanisms *Int. J. Robot. Res.* **28** 285–302
- [27] Chen Y, Grezmak J E, Graf N and Daltorio K 2022 Sideways crab-walking is faster and more efficient than forward walking for a hexapod robot *Bioinspiration Biomimetics* **17** 046001
- [28] Krummel G, Kaipa K N and Gupta S K 2014 A horseshoe crab inspired surf zone robot with righting capabilities *Int. Design Engineering Technical Conf. and Computers and Information in Engineering Conf.* vol 46360 (American Society of Mechanical Engineers) p V05AT08A010
- [29] Birch D W 1979 Food Preferences of Hemigrapsus Nudus (Dana, 1851) (Decapoda, Grapsidae) On San Juan Island, Washington, USA *Crustac* **36** 186–8
- [30] Knudsen J W 1964 Observations of the reproductive cycles and ecology of the common Brachyura and crablike Anomura of Puget Sound *Pac. Sci.* **XVIII**
- [31] McLaughlin P A and Lemaitre R 1997 Carcinization in the Anomura—fact or fiction? I. Evidence from adult morphology *Contrib. Zool.* **67** 79–123
- [32] Keiler J, Wirkner C S and Richter S 2017 One hundred years of carcinization—the evolution of the crab-like habitus in Anomura (Arthropoda: Crustacea) *Biol. J. Linn. Soc.* **121** 200–22
- [33] Tsang L M, Chan T, Ah Yong S T and Chu K H 2011 Hermit to king, or hermit to all: multiple transitions to crab-like forms from hermit crab ancestors *Syst. Biol.* **60** 616–29
- [34] Watson-Zink V M September 2021 Making the grade: physiological adaptations to terrestrial environments in decapod crabs *Arthropod Struct. Dev.* **64** 101089
- [35] Wolfe J M, Luque J and Bracken-Grissom H D 2021 How to become a crab: phenotypic constraints on a recurring body plan *Bioessays* **43** e2100020
- [36] Vidal-Gadea A G, Rinehart M D and Belanger J H 2008 Skeletal adaptations for forwards and sideways walking in three species of decapod crustaceans *Arthropod Struct. Dev.* **37** 95–108
- [37] Ritzmann R E, Quinn R D and Fischer M S 2004 Convergent evolution and locomotion through complex terrain by insects, vertebrates and robots *Arthropod Struct. Dev.* **33** 361–79
- [38] Grezmak J, Graf N, Behr A and Daltorio K 2021 Terrain classification based on sensed leg compliance for amphibious crab robot *IEEE Sensors J.* **21** 23308–16
- [39] Sartoretti G, Paivine W, Shi Y, Wu Y and Choset H 2019 Distributed learning of decentralized control policies for articulated mobile robots *IEEE Trans. Robot.* **35** 1109–22
- [40] Graf N M, Behr A M and Daltorio K A 2021 Dactyls and inward gripping stance for amphibious crab-like robots on sand *Bioinspiration Biomimetics* **16** 026021
- [41] Hutter M *et al* 2016 Anymal—a highly mobile and dynamic quadrupedal robot 2016 *IEEE/RSJ Int. Conf. Intelligent Robots and Systems (IROS)* (Piscataway, NJ: IEEE) pp 38–44
- [42] Jayaram K and Full R J 2016 Cockroaches traverse crevices, crawl rapidly in confined spaces, and inspire a soft, legged robot *Proc. Natl Acad. Sci.* **113** E950–7
- [43] Chong B *et al* 2022 A general locomotion control framework for multi-legged locomotors *Bioinspiration Biomimetics* **17** 046015
- [44] Raibert M, Blankespoor K, Nelson G and Playter R 2008 Bigdog, the rough-terrain quadruped robot *IFAC Proc. Vol.* **41** 10822–5
- [45] Katz B, Carlo J D and Kim S 2019 Mini cheetah: a platform for pushing the limits of dynamic quadruped control 2019 *Int. Conf. Robotics and Automation (ICRA)* pp 6295–301
- [46] Michael K 2012 Meet Boston dynamics' LS3—the latest robotic war machine *The Conversation*
- [47] Park H W, Wensing P M and Kim S 2021 Jumping over obstacles with MIT cheetah 2 *Robot. Autonom. Syst.* **136** 103703
- [48] BDI Spot Mini 2008 Boston dynamics Retrieve from <http://bostondynamics.com>
- [49] Shi F, Homberger T, Lee J, Miki T, Zhao M, Farshidian F, Okada K, Inaba M and Hutter M 2021 Circus anymal: a quadruped learning dexterous manipulation with its limbs 2021 *IEEE Int. Conf. Robotics and Automation (ICRA)* (Piscataway, NJ: IEEE) pp 2316–23
- [50] Lin Y, Tian Y, Xue Y, Han S, Zhang H, Lai W and Xiao X 2021 Innovative design and simulation of a transformable robot with flexibility and versatility, RHex-T3 2021 *IEEE Int. Conf. Robotics and Automation (ICRA)* (Institute of Electrical and Electronics Engineers Inc.) pp 6992–8
- [51] Schroer R T, Boggess M J, Bachmann R J, Quinn R D and Ritzmann R E 2004 Comparing cockroach and Whlegs robot body motions *IEEE Int. Conf. Robotics and Automation 2004. Proc. ICRA'04. 2004* vol 4 (Piscataway, NJ: IEEE) pp 3288–93
- [52] Woolley R, Timmis J and Tyrrell A M 2021 Cylindabot: transformable Whleg robot traversing stepped and sloped environments *Robotics* **10** 104
- [53] Quinn R D 2012 Whlegs retrieve from <https://engineering.case.edu/groups/biorobots/whlegs>
- [54] Kim Y S, Jung G P, Kim H, Cho K J and Chu C N 2014 Wheel transformer: a wheel-leg hybrid robot with passive transformable wheels *IEEE Trans. Robot.* **30** 1487–98
- [55] Belli I, Poverini M P, Laurenzi A, Hoffman E M, Rocco P and Tsagarakis N G 2021 Optimization-based quadrupedal hybrid wheeled-legged locomotion 2020 *IEEE-RAS 20th Int. Conf. Humanoid Robots (Humanoids)* (Piscataway, NJ: IEEE) pp 41–6

- [56] Bjelonic M, Sankar P K, Bellicoso C D, Vallery H and Hutter M 2020 Rolling in the deep—hybrid locomotion for wheeled-legged robots using online trajectory optimization *IEEE Robot. Autom. Lett.* **5** 3626–33
- [57] Sanchez E S 2018 Rowdy runner II: an independently actuated rimless wheel robot PhD Thesis The University of Texas at San Antonio
- [58] Dynamics Boston 2017 Introducing handle Youtube link <https://youtube.com/watch?v=-7xvqQeoA8c>
- [59] Semini C, Goldsmith J, Rehman B U, Frigerio M, Barasuol V, Focchi M and Caldwell D G 2015 Design overview of the hydraulic quadruped robots *The 14th Scandinavian Int. Conf. Fluid Power* (Tampere University of Technology) pp 20–2
- [60] Zhou J, Nguyen Q, Kamath S, Hacohen Y, Zhu C, Fu M J and Daltorio K A 2022 Hands to hexapods, wearable user interface design for specifying leg placement for legged robots *Front. Robot. AI* **99** 852270
- [61] She Y, Hurd C J and Su H J 2015 A transformable wheel robot with a passive leg *2015 IEEE/RSJ Int. Conf. Intelligent Robots and Systems (IROS)* (Piscataway, NJ): IEEE) pp 4165–70
- [62] Lambrecht B G A, Horchler A D and Quinn R D 2005 A small, insect-inspired robot that runs and jumps *Proc. 2005 IEEE Int. Conf. Robotics and Automation* (Piscataway, NJ: IEEE) pp 1240–5
- [63] Engineers Edge 2000 Coefficient of friction equation and table chart retrieve from https://engineersedge.com/coefficients_of_friction.htm
- [64] Roymech.org 2020 Coefficients of friction retrieve from https://roymech.org/Useful_Tables/Tribology/co_of_fric.html
- [65] Lynch G A, Rome L and Koditschek D E 2011 Sprawl angle in simplified models of vertical climbing: implications for robots and roaches *Appl. Bionics Biomech.* **8** 441–52
- [66] Taylor J R A 2018 Aquatic versus terrestrial crab skeletal support: morphology, mechanics, molting and scaling *J. Exp. Biol.* **221** jeb185421
- [67] Abramoff M D, Magalhães P J and Ram S J 2004 Image processing with imagej *Biophoton. Int.* **11** 36–42
- [68] Martinez M M, Full R J and Koehl M A 1998 Underwater punting by an intertidal crab: a novel gait revealed by the kinematics of pedestrian locomotion in air versus water *J. Exp. Biol.* **201** 2609–23
- [69] Hui C A 1992 Walking of the shore crab *pachygrapsus crassipes* in its two natural environments *J. Exp. Biol.* **165** 213–27
- [70] Perry B 2007 Crab leg segment length as a variation of environmental specialization *Technical Report* (Oregon Institute of Marine Biology)
- [71] Vidal-Gadea A G, Rinehart M D and Belanger J H March 2008 Skeletal adaptations for forwards and sideways walking in three species of decapod crustaceans *Arthropod Struct. Dev.* **37** 95–108
- [72] Belanger J 2013 Appendage diversity and modes of locomotion *The Natural History of the Crustacea* vol 1 pp 261–75
- [73] Graf N M, Grezmak J E and Daltorio K A 2022 Get a grip: inward dactyl motions improve efficiency of sideways-walking gait for an amphibious crab-like robot *Bioinspiration Biomimetics*
- [74] Bainbridge J 2017 *3D printing filament properties* <https://github.com/superjamie/lazyweb/wiki/3D-Printing-Filament-Properties>
- [75] Perepelkina S, Kovalenko P, Pechenko R and Makhmudova K 2017 Investigation of friction coefficient of various polymers used in rapid prototyping technologies with different settings of 3D printing *Tribol. Ind.* **39** 519